

Article

Performance Analysis of a Proton Exchange Membrane Fuel Cell Based Syngas

Xiuqin Zhang ¹, Qiubao Lin ¹, Huiying Liu ¹, Xiaowei Chen ¹, Sunqing Su ¹ and Meng Ni ^{2,*} 

¹ Department of Physics, Jimei University, Xiamen 361021, China; yoshow520@126.com (X.Z.); qblin@jmu.edu.cn (Q.L.); hylu@jmu.edu.cn (H.L.); xwchen@jmu.edu.cn (X.C.); sqsu@jmu.edu.cn (S.S.)

² Department of Building and Real Estate, The Hong Kong Polytechnic University, Hong Kong, China

* Correspondence: bsmengni@polyu.edu.hk; Tel.: +852-27664152; Fax: +852-27645131

Received: 31 October 2018; Accepted: 5 January 2019; Published: 18 January 2019



Abstract: External chemical reactors for steam reforming and water gas shift reactions are needed for a proton exchange membrane (PEM) fuel cell system using syngas fuel. For the preheating of syngas and stable steam reforming reaction at 600 °C, residual hydrogen from a fuel cell and a certain amount of additional syngas are burned. The combustion temperature is calculated and the molar ratio of the syngas into burner and steam reformer is determined. Based on thermodynamics and electrochemistry, the electric power density and energy conversion efficiency of a PEM fuel cell based syngas are expressed. The effects of the temperature, the hydrogen utilization factor at the anode, and the molar ratio of the syngas into burner and steam reformer on the performance of a PEM fuel cell are discussed. To achieve the maximum power density or efficiency, the key parameters are determined. This manuscript presents the detailed operating process of a PEM fuel cell, the allocation of the syngas for combustion and electric generation, and the feasibility of a PEM fuel cell using syngas.

Keywords: PEM fuel cell; syngas; steam reforming; combustion; performance analysis

1. Introduction

The hydrogen fuel cell is a promising technology for electric vehicle applications [1]. Compared with battery-based electric vehicles, hydrogen fuel cell-based electric vehicles can easily deliver a much higher range, and the fueling of hydrogen only takes a few minutes. However, it is still challenging to store hydrogen in vehicles with small volume and mass. The currently used hydrogen cylinder is bulky while the metal hydride is relatively heavy. One option to solve the hydrogen storage problem is to supply hydrogen onboard by the steam reforming of ethanol [2,3] or diesel [4]. This option has been demonstrated to be feasible and is practically used. However, hydrogen production from nonrenewable resources results in pollutant emission from the life cycle point of view. Biomass is an important renewable resource and is carbon neutral. The use of biomass-derived fuel in fuel cell vehicles can achieve green transportation with minimal pollutant emission. When biomass-derived fuel is used in a proton exchange membrane (PEM) fuel cell, the syngas production [5], steam reforming, and water gas shift reactions are most necessary to provide pure hydrogen. Although a recent study showed that it is possible to directly use biomass in a fuel cell without converting biomass into hydrogen rich gases [6], the power density is too low for practical applications. Two conversion paths, anaerobic digestion and gasification, are available to convert biomass into hydrogen-rich gases, which contains hydrogen, methane, carbon monoxide, carbon dioxide, and other gases [7]. As methane cannot be electrochemically oxidized in the PEM fuel cell and the carbon monoxide can easily poison the noble metal catalyst in the fuel cell, the further steam reforming and the water gas shift are necessary to convert the residual methane and carbon monoxide to hydrogen, respectively.

As the steam reforming reaction is endothermic, the addition of CaO into glycerol steam reforming is proposed [8], since the conversion of CaO into CaCO₃ can provide enough heat for the endothermic reaction. However, the new product CaCO₃ may cover the catalyst of the steam reforming reaction and thus limits the long-term durability. The high-temperature exhaust heat from a Stirling engine can be used for steam reforming [9], but the operation of the PEM fuel cell is dependent on the engine.

It is better if the steam reforming and the combustion of residual hydrogen from a PEM fuel cell are integrated. The combustion of residual fuel from a fuel cell and directly fed fuel of a burner can generate enough heat for the reforming [10]. A membrane reactor of reforming is employed for the improvement of the system efficiency [11]. The effect of the molar ratio of steam and hydrocarbon on the steam reforming product [12] and system efficiency [13] is present. The molar ratio of the fuel into the burner and steam reformer has almost not been discussed, and it is considered as a parameter in this paper which will affect the performance of the system.

To improve the performance of a PEM fuel cell, various strategies have been proposed. A gas diffusion layer with micropores of the PEM fuel cell is suggested [14] because the low thermal conductivity of it can accelerate the transportation of water while the operating temperature of the fuel cell may be unstable. The addition of silicates to the proton exchange membrane will improve the thermal conductivity, water uptake, and proton conductivity of the membrane [15]. The work in Reference [16] exhibits high water uptake and proton conductivity of the activated carbon/Nafion hybrid composite. The ohmic polarization loss is influenced by the proton conductivity and gas humidity [17]. If there is analytic relation between the proton conductivity and composition of the membrane, the performance of a PEM fuel cell can be optimized. The concentration polarization loss mainly occurs in the cathode [18]. The flow field of the bipolar plate is designed to reduce the loss [19]. The mathematical expressions of activation, ohm, and concentration overpotentials in engineering are used in this study.

2. The Auxiliary Systems outside a PEM Fuel Cell

The schematic diagram of the system is shown in Figure 1, where the syngas and water are preheated from 25 °C to 600 °C in heat exchanger 1 (HE1); the steam reforming reaction of methane and water vapor in the gases is taken place in heat exchanger 2 (HE2); and the carbon monoxide is eliminated after passing the high-temperature water gas shift (HTS), the low-temperature water gas shift (LTS), and the preferential oxidation reactions (PROX). The air flowing into the cathode of a fuel cell is preheated by the gases leaving the fuel cell in heat exchanger 3 (HE3). The residual hydrogen leaving the anode of a fuel cell and a certain amount of additional syngas are burned in the after burner (AB); the high-temperature combustion product is used to supply enough heat for the preheating and steam reforming reactions in HE1 and HE2, respectively.

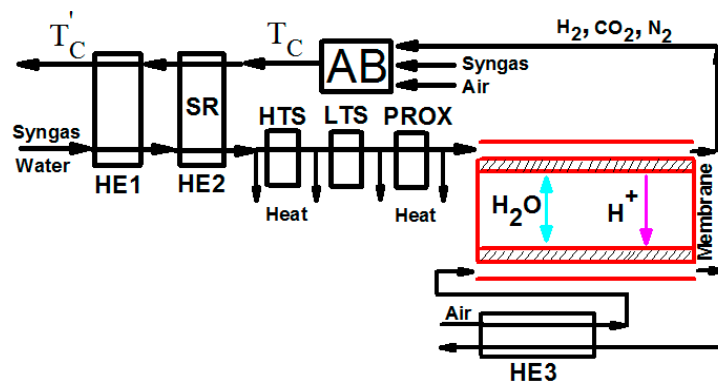
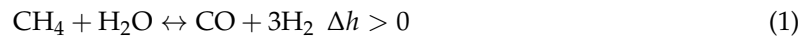


Figure 1. The schematic diagram of a proton exchange membrane (PEM) fuel cell based syngas, where abbreviations of HE1, HE2, and HE3 are heat exchangers, SR is a steam reformer, HTS and LTS are water gas shift reactions, PROX is a preferential oxidizer, and AB is an auxiliary burner.

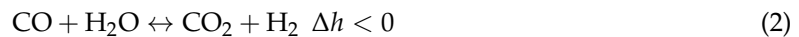
2.1. The Heat Needed in HE1 and HE2

The water gas shift and preferential oxidation reactions are exothermic; the heat about them will not be discussed. Assuming the heat released from the residual air and water leaving the cathode is enough for the preheating of air flowing into the fuel cell, the process of heat transfer in HE3 will also not be discussed.

If the mole flow rate of syngas into HE1 is n ($\text{mol}\cdot\text{s}^{-1}$) and the amount of water in the flow is twice of that needed for the steam reforming and water gas shift reactions, the steam reforming and water gas shift reactions are, respectively,



and



where Δh is the enthalpy change of gases if one mole CH_4 is consumed in Equation (1) or one mole CO is consumed in Equation (2). The mole rate of water added in the syngas is

$$n_{\text{H}_2\text{O}} = 2n(2x_{\text{CH}_4} + x_{\text{CO}}) - nx_{\text{H}_2\text{O}}, \quad (3)$$

where x_k is the mole fraction of k in the syngas; the specific components of the syngas are shown in Table 1 [20]. The heat needed for the preheating of the syngas and water is

$$\dot{Q}_1 = n \sum_k (x_k \int_{298.15}^{873.15} C_{k,m} dt) + n_{\text{H}_2\text{O}} \int_{298.15}^{873.15} C_{\text{H}_2\text{O},m} dt + 2n(2x_{\text{CH}_4} + x_{\text{CO}})L_{\text{H}_2\text{O},m}, \quad (4)$$

where $C_{k,m}$ is the molar heat capacity of k , the value of which is shown in Table 2 [21,22]; t is temperature; and $L_{\text{H}_2\text{O},m}$ is the latent heat of one mole water. The heat needed for the steam reforming reaction is

$$\dot{Q}_2 = nx_{\text{CH}_4}(3h_{\text{H}_2} + h_{\text{CO}} - h_{\text{CH}_4} - h_{\text{H}_2\text{O}}), \quad (5)$$

where h_k is the enthalpy of k per mole at 600 °C and 1atm and is calculated as

$$h_k = h_k^0 + \int_{298.15}^{873.15} C_{k,m} dt, \quad (6)$$

where h_k^0 is the enthalpy of k per mole at 25 °C and 1 atm, the value of which is shown in Table 2.

Table 1. The composition of syngas [20].

Component k	H ₂	CH ₄	CO	CO ₂	H ₂ O	N ₂
Mole fraction of k in syngas: x_k	0.13	0.01	0.16	0.05	0.36	0.29

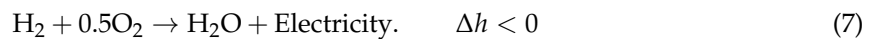
Table 2. Thermodynamic parameters of the chemical components [21,22], where (g) and (l) refer to gas and liquid phases, respectively.

Component k	h_k^0 (J·mol ⁻¹)	s_k^0 (J·mol ⁻¹ ·K ⁻¹)	$L_{\text{H}_2\text{O},m}$ (J·mol ⁻¹)	Molar Heat Capacity $C_{k,m}$ (J·mol ⁻¹ ·K ⁻¹)
N ₂	0	—	—	29.12
O ₂	0	205.138	—	25.8911 + 0.0129874t - 0.0000038644t ²
CH ₄	-75,000	—	—	14.1555 + 0.0755466t - 0.0000180032t ²
CO ₂	-393,800	—	—	26.0167 + 0.0435259t - 0.0000148422t ²
CO	-110,500	—	—	26.8742 + 0.006971t - 0.0000008206t ²
H ₂	0	130.695	—	29.0856 - 0.0008373t + 0.0000020138t ²
H ₂ O (g)	-241,800	—	—	30 + 0.01071t + 33000/t ²
H ₂ O (l)	-285,800	69.940	40,700	75.44

2.2. The Molar Ratio of Syngas into the Burner and Steam Reformer

The relative low temperature of a PEM fuel cell will reduce the cost of materials and will present a short start time and a fast transient response [23]. In this paper, the working temperature of the PEM fuel cell is under 100 °C and the water can be separated from the gases which will enter into the anode of the fuel cell. If CO is reacted fully in the water gas shift reactions, the gases flowing into the fuel cell is composed of H₂, CO₂, and N₂ by combining Equations (1) and (2).

The total electrochemical reaction in a fuel cell is

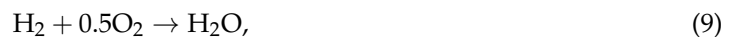


If the hydrogen utilization factor at the anode is u_{H_2} , the mole flowing rate of residual hydrogen is determined, and the total enthalpy of residual H₂, CO₂, and N₂ leaving the fuel cell is

$$\dot{H}_{cell} = n(x_{\text{H}_2} + 4x_{\text{CH}_4} + x_{\text{CO}})(1 - u_{\text{H}_2})h_{\text{H}_2}(T) + n(x_{\text{CO}_2} + x_{\text{CH}_4} + x_{\text{CO}})h_{\text{CO}_2}(T) + nx_{\text{N}_2}h_{\text{N}_2}(T), \quad (8)$$

where $h_k(T)$ is the enthalpy of k per mole at temperature T and 1 atm.

The combustion of residual hydrogen may not be enough for the preheating and steam reforming of the syngas, so extra syngas is added in the burner. The combustion equations in the burners are, respectively,



and



Assuming the molar ratio of the syngas into the burner and steam reformer is x and the air in the burner is just enough for the combustion, the enthalpy of gases flowing into the burner unit time is

$$\begin{aligned} \dot{H}_{in} = & \dot{H}_{cell} + nx \sum_k x_k h_k^0 + \\ & \frac{1}{2}n[(x_{\text{H}_2} + 4x_{\text{CH}_4} + x_{\text{CO}})(1 - u_{\text{H}_2}) + xx_{\text{H}_2} + xx_{\text{CO}} + 4xx_{\text{CH}_4}](h_{\text{O}_2}^0 + \frac{78}{21}h_{\text{N}_2}^0) \end{aligned} \quad (12)$$

Combining Equations (8)–(12), the component of the combustion product is determined. If the combustion temperature is T_C , one can obtain the enthalpy of gases leaving the burner as

$$\begin{aligned} \dot{H}_{out} = & n[(x_{\text{H}_2} + 4x_{\text{CH}_4} + x_{\text{CO}})(1 - u_{\text{H}_2}) + xx_{\text{H}_2} + xx_{\text{H}_2\text{O}} + 2xx_{\text{CH}_4}]h_{\text{H}_2\text{O}}(T_C) + \\ & n(1 + x)(x_{\text{CO}_2} + x_{\text{CH}_4} + x_{\text{CO}})h_{\text{CO}_2}(T_C) + n(1 + x)x_{\text{N}_2}h_{\text{N}_2}(T_C) + \frac{1}{2}n[(x_{\text{H}_2} + 4x_{\text{CH}_4} + x_{\text{CO}})(1 - u_{\text{H}_2}) + \\ & xx_{\text{H}_2} + xx_{\text{CO}} + 4xx_{\text{CH}_4}]\frac{78}{21}h_{\text{N}_2}(T_C). \end{aligned} \quad (13)$$

Assuming the burner is adiabatic, the enthalpy of gases flowing into the burner is equal to that leaving the burner:

$$\dot{H}_{in} = \dot{H}_{out}. \quad (14)$$

Combining Equations (8) and (12)–(14), x is a function of u_{H_2} , T , and T_C . T_C is not random; it should be larger than 600 °C, and the heat released by the combustion product must be enough for the preheating and steam reforming reaction in HE1 and HE2 as

$$\begin{aligned} & n[(x_{\text{H}_2} + 4x_{\text{CH}_4} + x_{\text{CO}})(1 - u_{\text{H}_2}) + xx_{\text{H}_2} + xx_{\text{H}_2\text{O}} + 2xx_{\text{CH}_4}](\int_{T_C}^{T_C} C_{\text{H}_2\text{O},m} dt + L_{\text{H}_2\text{O},m}) + \\ & n(1 + x)(x_{\text{CO}_2} + x_{\text{CH}_4} + x_{\text{CO}}) \int_{T_C}^{T_C} C_{\text{CO}_2,m} dt + n(1 + x)x_{\text{N}_2} \int_{T_C}^{T_C} C_{\text{N}_2,m} dt + \\ & \frac{1}{2}n[(x_{\text{H}_2} + 4x_{\text{CH}_4} + x_{\text{CO}})(1 - u_{\text{H}_2}) + xx_{\text{H}_2} + xx_{\text{CO}} + 4xx_{\text{CH}_4}]\frac{78}{21} \int_{T_C}^{T_C} C_{\text{N}_2,m} dt \geq \dot{Q}_1 + \dot{Q}_2, \end{aligned} \quad (15)$$

where T'_C is the temperature of the combustion product leaving HE1. If the rate of heat released from the combustion product is as close to that needed for the preheating and steam reforming reaction as possible, Equation (15) is another relationship between x , u_{H_2} , T , and T_C .

Combining Equations (3)–(6), (8), and (12)–(15), x and T_C are both independent of n , while they are functions of u_{H_2} , T , and T'_C . If T and T'_C are given, one can obtain the curves of x and T_C varying with u_{H_2} as shown in Figures 2 and 3, respectively. If the hydrogen utilization factor is smaller, there are more residual hydrogen leaving the fuel cell, the combustion temperature is higher, and the amount of syngas in the burner is less as shown in Figures 2 and 3, so the cost of the steam reforming reaction is lower. However, the hydrogen utilization factor at the anode of a fuel cell will affect the electric power of the fuel cell [24]; there is a specific hydrogen utilization factor under the maximum electric power. The energy conversion efficiency is dependent on both the amount of syngas in the burner and the electric power need to be introduced and optimized. Figures 2 and 3 also show that if the working temperature of the PEM fuel cell is higher, the temperature of the combustion product is higher and the amount of syngas needed for the burner is less.

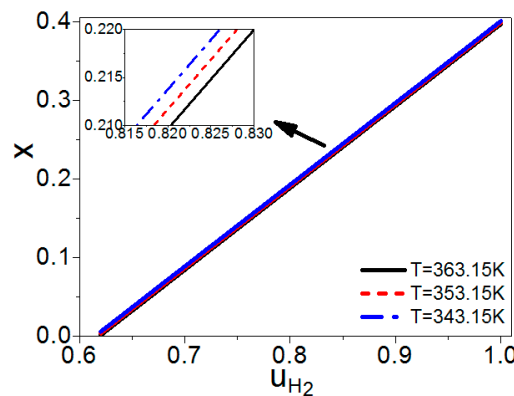


Figure 2. Curves of x varying with u_{H_2} , where $T'_C = 30\text{ }^\circ\text{C}$.

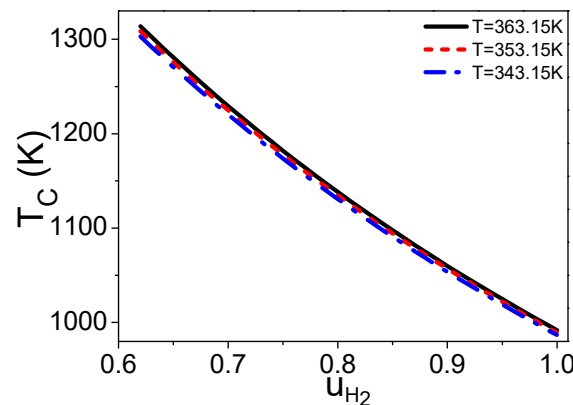


Figure 3. Curves of T_C varying with u_{H_2} , where $T'_C = 30\text{ }^\circ\text{C}$.

3. The Electric Power of a PEM Fuel Cell Based Syngas

As defined above, the molar rate of the hydrogen used in Equation (7) is

$$n(x_{H_2} + 4x_{CH_4} + x_{CO})u_{H_2}. \tag{16}$$

According to thermodynamics, the available energy released by the reaction is

$$n(x_{H_2} + 4x_{CH_4} + x_{CO})u_{H_2}\Delta g(T), \tag{17}$$

where $\Delta g(T)$ is the Gibbs function change of the gases if one molar hydrogen is consumed in Equation (7), and it can be calculated as

$$\Delta g(T) = \Delta h(T) - T\Delta s(T), \quad (18)$$

where $\Delta h(T)$ and $\Delta s(T)$ are, respectively, the enthalpy and entropy changes of the gases if one molar hydrogen is consumed in Equation (7). The enthalpy change of the gases is

$$\Delta h(T) = h_{\text{H}_2\text{O}}(T) - h_{\text{H}_2}(T) - 0.5h_{\text{O}_2}(T). \quad (19)$$

The entropy change of the gases is

$$\Delta s(T) = s_{\text{H}_2\text{O}}^0 + \int_{298.15}^T \frac{C_{\text{H}_2\text{O,m}}}{T} dt - (s_{\text{H}_2}^0 + \int_{298.15}^T \frac{C_{\text{H}_2,m}}{T} dt) - 0.5(s_{\text{O}_2}^0 + \int_{298.15}^T \frac{C_{\text{O}_2,m}}{T} dt) + R \ln \frac{p_{\text{H}_2} p_{\text{O}_2}^{0.5}}{p_{\text{H}_2\text{O}}}, \quad (20)$$

where s_k^0 is the entropy of per mole k at 25 °C and 1 atm; R is the universal gas constant; p_k is the partial pressure of k at the electrode; the partial pressure of liquid water is 1;

$$p_{\text{H}_2} = p_a \left(1 - \frac{p_s}{p_a}\right) / \left[1 + \frac{x_a}{2} \left(1 + \frac{\delta_a}{\delta_a - 1}\right)\right]; \quad (21)$$

and

$$p_{\text{O}_2} = p_c \left(1 - \frac{p_s}{p_c}\right) / \left[1 + \frac{x_c}{2} \left(1 + \frac{\delta_c}{\delta_c - 1}\right)\right], \quad (22)$$

where p_a (atm) and p_c (atm) are pressures at anode and cathode, respectively [25], p_s (atm) is the saturation pressure of water and is dependent on the temperature [26], x_a and x_c are dry gas molar ratios at anode and cathode, respectively, and δ_a and δ_c are stoichiometry coefficients.

As shown by the equivalent circuit of a PEM fuel cell in Ref. [27], there is internal resistance of a fuel cell. The heat produced by the internal resistance is

$$I(V_{act} + V_{ohm} + V_{con}), \quad (23)$$

where I is the intensity of the electric current of the PEM fuel cell and V_{act} is the activation overpotential. The general expression of it is the Butler–Vollmer equation [28]. There is another pattern reported by Tafel [29] based on the results of the experiments and is defined as

$$V_{act} = \frac{RT}{n_e F} \frac{(\alpha_a + \alpha_c)}{\alpha_a \alpha_c} \ln \frac{i}{i_0}, \quad (24)$$

where n_e is the number of electrons transferred through the external circuit if one molecule of hydrogen is reacted; F is Faraday's constant; α_a and α_c represent the anode and cathode charge transfer coefficients; $i = I/A_c$ is the current density of the PEM fuel cell; A_c is the effective surface area of the bipolar plate; i_0 is the exchange current density of the electrodes [30] and is defined as

$$i_0 = 1.27 \times 10^{-8} \exp(2.06 p_{\text{O}_2}); \quad (25)$$

and V_{ohm} and V_{con} are ohm and concentration overpotentials [31]. The expressions of them are [27]

$$V_{ohm} = i \frac{\delta_{mem}}{\sigma_{mem}} \quad (26)$$

and

$$V_{con} = i \left(\beta_1 \frac{i}{i_L}\right)^{\beta_2}, \quad (27)$$

respectively, where δ_{mem} is the thickness of membrane and σ_{mem} is the membrane conductivity [27]. It can be defined as

$$\sigma_{mem} = (0.005139\mu_{mem} - 0.003260) \exp\left[1268\left(\frac{1}{303} - \frac{1}{T}\right)\right], \quad (28)$$

where μ_{mem} is the water content and is determined by water vapor activity, i_L is the limiting current density, β_1 is dependent on the partial pressure of oxygen and the temperature at the cathode [30], and β_2 is constant.

According to energy conservation, the electric power of a PEM fuel cell is

$$P_e = -n(x_{H_2} + 4x_{CH_4} + x_{CO})u_{H_2}\Delta g(T) - I(V_{act} + V_{ohm} + V_{con}). \quad (29)$$

Based on Faraday's law, the intensity of the electric current in Equation (29) can be presented as

$$I = n(x_{H_2} + 4x_{CH_4} + x_{CO})u_{H_2}n_eF. \quad (30)$$

Combining Equations (18)–(30) and Table 3 [25,30,32], the electric power density " $P_e^* = P_e/A_c$ " is dependent on " $n^* = n/A_c$ ", u_{H_2} , and T . If T is given, one can obtain the maximum power density varying with n^* by optimizing the hydrogen utilization factor, as shown by the solid curve in Figure 4. The hydrogen utilization factor under the maximum power density is shown by the solid curve in Figure 5. There is a certain electric current density under the maximum power density of the PEM fuel cell [24]. This means that there is an optimal product of n^* and u_{H_2} from Equation (30). When n^* is smaller than $0.17 \text{ (mol}\cdot\text{s}^{-1}\cdot\text{m}^{-2})$, the product of n^* and u_{H_2} is always smaller than the optimum value, even though $u_{H_2} = 1$ in Figure 5 and the electric power density of the PEM fuel cell is a monotonous increasing function of the molar flow rate of the syngas in Figure 4. When $n^* \geq 0.17 \text{ (mol}\cdot\text{s}^{-1}\cdot\text{m}^{-2})$, the hydrogen utilization factor is decreasing with the increase of the molar flow rate of syngas to reach the optimal product of them in Figure 5, and the electric power density is constant in Figure 4.

Table 3. Parameters used in the system.

Parameter	Value
Number of electrons, n_e	2
Faraday constant, $F \text{ (C mol}^{-1})$	96485
Universal gas constant, $R \text{ (J}\cdot\text{mol}^{-1}\cdot\text{K}^{-1})$	8.314
Pressure at the anode, $p_a \text{ (atm)}$	3 [13]
Pressure at the cathode, $p_c \text{ (atm)}$	5 [13]
Anode stoichiometry, δ_a	1.5 [20]
Cathode stoichiometry, δ_c	3 [20]
Dry gas molar ratio at anode, x_a	$(x_{N_2} + x_{CO_2} + x_{CH_4} + x_{CO}) / (x_{H_2} + x_{CO} + 4x_{CH_4})$ [13]
Dry gas molar ratio at cathode, x_c	3.762 (air)
Charge transfer coefficient at the anode, α_a	0.5 [20]
Charge transfer coefficient at the cathode, α_c	1 [20]
Membrane thickness, $\delta_{mem} \text{ (cm)}$	0.018 [13]
μ_{mem}	14 [21]
Constant, β_2	2 [20]
Limiting current density, $i_L \text{ (A cm}^{-2})$	2 [20]
$T = 70 \text{ }^\circ\text{C}$: $p_s \text{ (atm)}$; β_1	0.3071; 0.2048
$q_{LHV} \text{ (kJ mol}^{-1})$: $k = H_2; CO; CH_4$	241.9; 283.2; 803.7

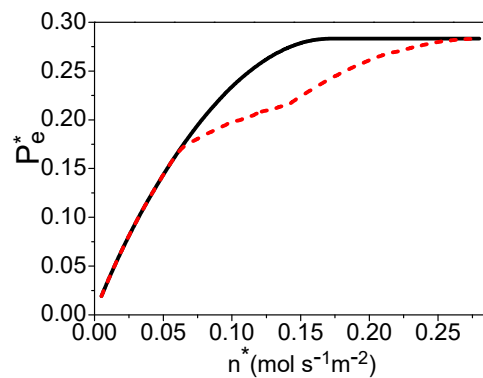


Figure 4. The power density varying with n^* , where $T = 70\text{ }^\circ\text{C}$ and $T'_C = 30\text{ }^\circ\text{C}$. The solid and dash curves are, respectively, the maximum power density and the power density under the maximum efficiency.

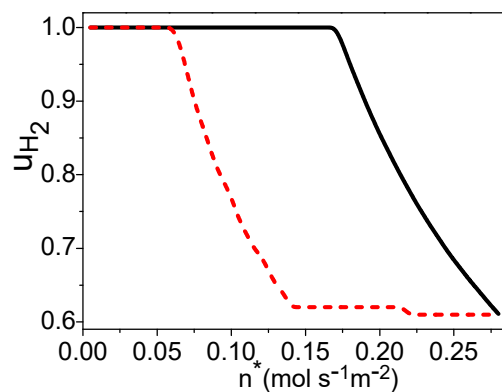


Figure 5. The hydrogen utilization factor varying with n^* , where $T = 70\text{ }^\circ\text{C}$ and $T'_C = 30\text{ }^\circ\text{C}$. The solid and dash curves are, respectively, the hydrogen utilization factor under the maximum power density and the maximum efficiency.

There is a linear relationship between x and u_{H_2} in Figure 2, so one can also obtain x under the maximum power density, as shown by the solid curve in Figure 6. The graphs of Figures 5 and 6 are similar. When there is no residual hydrogen from the fuel cell, the molar ratio of the syngas into the burner and steam reformer is 0.4. As the amount of residual hydrogen increases, the molar ratio x is decreasing. When the hydrogen utilization factor is about 0.61, there is no need to add syngas into the burner. As discussed in Section 2.2, the total energy conversion efficiency of the hybrid system of a PEM fuel cell and steam reformer is dependent on the hydrogen utilization factor at the anode of the fuel cell, so the efficiency of the hybrid system will be further optimized.

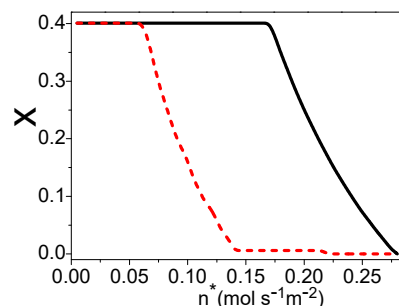


Figure 6. Curves of x varying with n^* , where $T = 70\text{ }^\circ\text{C}$ and $T'_C = 30\text{ }^\circ\text{C}$. The solid and dash curves are x under the maximum power density and the maximum efficiency, respectively.

4. The Total Energy Conversion Efficiency

The energy conversion efficiency of the hybrid system of a PEM fuel cell and steam reformer is

$$\eta = \frac{P_e}{(1+x)(x_{\text{H}_2}q_{\text{LHV}}(\text{H}_2)+x_{\text{CO}}q_{\text{LHV}}(\text{CO})+x_{\text{CH}_4}q_{\text{LHV}}(\text{CH}_4))} = \frac{(x_{\text{H}_2}+4x_{\text{CH}_4}+x_{\text{CO}})u_{\text{H}_2}[-\Delta g(T)-n_e F(V_{\text{act}}+V_{\text{ohm}}+V_{\text{con}})]}{(1+x)(x_{\text{H}_2}q_{\text{LHV}}(\text{H}_2)+x_{\text{CO}}q_{\text{LHV}}(\text{CO})+x_{\text{CH}_4}q_{\text{LHV}}(\text{CH}_4))} \quad (31)$$

where $q_{\text{LHV}}(\text{k})$ is the lower heating value of per molar k. Combining Equations (18)–(31), η is dependent on n^* , u_{H_2} , x , and T , while there is a linear relationship between u_{H_2} and x . If temperature T is given, one can obtain the maximum efficiency varying with the molar flowing rate of the syngas by optimizing the hydrogen utilization factor in the fuel cell, as shown by the dash curve in Figure 7. The electric power density, hydrogen utilization factor, and x under the maximum efficiency are, respectively, shown by the dash curves in Figures 4–6. If the values of u_{H_2} and x derived in Section 3 are substituted into Equation (31), one can obtain the efficiency under the maximum power density as shown by the solid curve in Figure 7. The efficiency of the system is decreasing with the increase of the molar flowing rate of syngas.

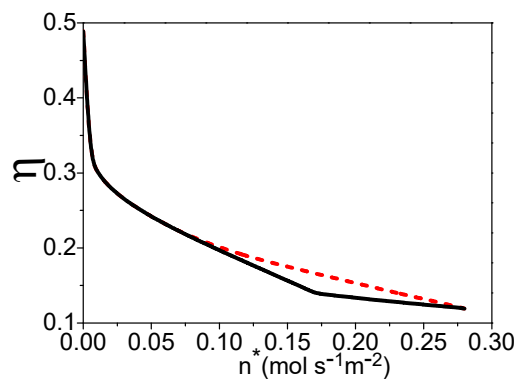


Figure 7. The efficiency varying with n^* , where $T = 70\text{ }^\circ\text{C}$ and $T'_C = 30\text{ }^\circ\text{C}$. The dash and solid curves are, respectively, the maximum efficiency and the efficiency under the maximum power density.

When n^* is smaller than $0.065\text{ (mol}\cdot\text{s}^{-1}\cdot\text{m}^{-2}\text{)}$, the working conditions of the maximum efficiency and the maximum power density are the same: The hydrogen should be reacted totally in the fuel cell, and the molar ratio of the syngas into the burner and steam reformer is 0.4. When $0.065 \leq n^* \leq 0.14\text{ (mol}\cdot\text{s}^{-1}\cdot\text{m}^{-2}\text{)}$, there should be residual hydrogen leaving the fuel cell and x is smaller than 0.4 for the maximum efficiency of the system. When n^* is larger than $0.14\text{ (mol}\cdot\text{s}^{-1}\cdot\text{m}^{-2}\text{)}$, the hydrogen utilization factor is constant and about 0.61; there is no need to add syngas into the burner.

5. Conclusions

A model of the PEM fuel cell based syngas is established, and the residual hydrogen leaving the fuel cell and extra syngas are burned in a burner to supply enough high-temperature heat for the steam reforming reaction. There is a linear relationship between the hydrogen utilization factor in the fuel cell and the molar ratio of the syngas into the burner and steam reformer; if the hydrogen utilization factor is higher, the molar ratio is larger, and vice versa. Based on the thermodynamics and electrochemistry, the expressions of the electric power and energy conversion efficiency of the system are derived. For the maximum power density or maximum efficiency of a PEM fuel cell based syngas, the optimal hydrogen utilization factor in the fuel cell and the molar ratio of the syngas into the burner and steam reformer are, respectively, determined. In the future, the waste heat from a PEM fuel cell and the water gas shift reactions can be considered to be utilized to improve the energy conversion efficiency of the PEM fuel cell.

Author Contributions: Conceptualization, X.Z., Q.L., H.L., X.C., and S.S.; software, X.Z.; Writing—review and editing, M.N. and X.Z.

Funding: This work was funded by the National Natural Science Foundation, grant number 11605073 and 51601068; Natural Science Foundation of Fujian Province, grant number 2017J05009; and Fujian Province for Distinguished Young Scholars, grant number B17164.

Conflicts of Interest: The authors declare no conflict of interest.

Nomenclature

A_c	Effective surface area of the bipolar plate
α_a	Charge transfer coefficient at anode
α_c	Charge transfer coefficient at cathode
β_1	Parameter in the expression of overpotential
β_2	Constant in the expression of overpotential
$C_{k,m}$	Molar heat capacity of k
Δh	Enthalpy change of gases
$\Delta h(T)$	Enthalpy change of gases
$\Delta g(T)$	Gibbs function change of gases
$\Delta s(T)$	Entropy change of gases
δ_a	Stoichiometry coefficient
δ_c	Stoichiometry coefficient
δ_{mem}	Membrane thickness
F	Faraday constant
η	Efficiency of the hybrid system
h_k	Molar enthalpy of k at 600 °C
h_k^0	Molar enthalpy of k at 25 °C
$h_k(T)$	Molar enthalpy of k at temperature T
\dot{H}_{cell}	Enthalpy of gases leaving the fuel cell
\dot{H}_{in}	Enthalpy of gases into burner
\dot{H}_{out}	Enthalpy of gases leaving the burner
I	Electric current of a PEM fuel cell
i_0	Exchange current density of the electrodes
i	Current density of a PEM fuel cell
i_L	Limiting current density of a PEM fuel cell
$L_{H_2O,m}$	Latent heat of one mole water
μ_{mem}	Water content
n	Mole flow rate of syngas into HE1
n_{H_2O}	Mole rate of water added into syngas
n^*	Mole flow rate of syngas into HE1 unit area
n_e	Number of electrons
P_e^*	Electric power density of a PEM fuel cell
P_e	Electric power of a PEM fuel cell
p_c	Pressure at the cathode
p_a	Pressure at the anode
p_s	Saturation pressure of water

p_k	Partial pressure of k at the electrode
\dot{Q}_2	The heat needed in HE2 unit time
\dot{Q}_1	The heat needed in HE1 unit time
$q_{LHV}(k)$	Lower heating value of k per molar
R	Universal gas constant
s_k^0	Molar entropy of k at 25°C
σ_{mem}	Membrane conductivity
T	Operating temperature of a PEM fuel cell
T_C	Combustion temperature
t	Temperature
T'_C	Temperature of gases leaving HE1
u_{H_2}	Hydrogen utilization factor in a fuel cell
V_{act}	Activation overpotential
V_{ohm}	Ohm overpotential
V_{con}	Concentration overpotential
x_c	Dry gas molar ratio at cathode
x_a	Dry gas molar ratio at anode
x	The molar ratio
x_k	Molar fraction of k in syngas

References

1. Brey, J.J.; Carazo, A.F.; Brey, R. Exploring the marketability of fuel cell electric vehicles in terms of infrastructure and hydrogen costs in Spain. *Renew. Sustain. Energy Rev.* **2018**, *82*, 2893–2899. [[CrossRef](#)]
2. Ham, S.W.; Jo, S.Y.; Dong, H.W.; Jeong, J.W. A simplified PEM fuel cell model for building cogeneration applications. *Energy Build.* **2015**, *107*, 213–225. [[CrossRef](#)]
3. Izurieta, E.M.; Adrover, M.E.; Pedernera, M.N.; López, E. Ethanol processor design for hydrogen production. Kinetic analysis and process integration. *Ind. Eng. Chem. Res.* **2018**, *57*, 13615–13626. [[CrossRef](#)]
4. Maximini, M.; Engelhardt, P.; Brenner, M.; Beckmann, F.; Moritz, O. Fast start-up of a diesel fuel processor for PEM fuel cells. *Int. J. Hydrog. Energy* **2014**, *39*, 18154–18163. [[CrossRef](#)]
5. Peng, W.X.; Wang, L.S.; Mirzaee, M.; Ahmadi, H.; Esfahani, M.J.; Fremaux, S. Hydrogen and syngas production by catalytic biomass gasification. *Energy Convers. Manag.* **2017**, *135*, 270–273. [[CrossRef](#)]
6. Zhao, X.; Liu, W.; Deng, Y.; Zhu, J.Y. Low-temperature microbial and direct conversion of lignocellulosic biomass to electricity: Advances and Challenges. *Renew. Sustain. Energy Rev.* **2017**, *71*, 268–282. [[CrossRef](#)]
7. Guan, T.; Chutichai, B.; Alvfors, P.; Arpornwichanop, A. Biomass-fuelled PEM FC systems: Evaluation of two conversion paths relevant for different raw materials. *Energy Convers. Manag.* **2015**, *106*, 1183–1191. [[CrossRef](#)]
8. Wess, R.; Nores-Pondal, F.; Laborde, M.; Giunta, P. Single stage H₂ production, purification, and heat supply by means of sorption-enhanced steam reforming of glycerol. A thermodynamic analysis. *Chem. Eng. Sci.* **2015**, *134*, 86–95. [[CrossRef](#)]
9. Shin'ya, O.; Itaru, T.; Shunsuke, K.; Akira, H.; Seizi, S. Exergy analysis of the woody biomass Stirling engine and PEM-FC combined system with exhaust heat reforming. *Int. J. Hydrog. Energy* **2008**, *33*, 2289–2299.
10. Purnima, P.; Jayanti, S. A high-efficiency, auto-thermal system for on-board hydrogen production for low temperature PEM fuel cells using dual reforming of ethanol. *Int. J. Hydrog. Energy* **2016**, *41*, 13800–13810. [[CrossRef](#)]
11. Salemme, L.; Menna, L.; Simeone, M.; Volpicelli, G. Energy efficiency of membrane-based fuel processors-PEM fuel cell systems. *Int. J. Hydrog. Energy* **2010**, *35*, 3712–3720. [[CrossRef](#)]
12. Comas, J.; Dieuzeide, M.; Baronetti, G.; Laborde, M.; Amadeo, N. Methane steam reforming and ethanol steam reforming using a Ni(II)-Al(III) catalyst prepared from lamellar double hydroxides. *Chem. Eng. J.* **2006**, *118*, 11–15. [[CrossRef](#)]
13. Ersoz, A.; Olgun, H.; Ozdogan, S. Reforming options for hydrogen production from fossil fuels for PEM fuel cells. *J. Power Sources* **2006**, *154*, 67–73. [[CrossRef](#)]

14. Ito, H.; Heo, Y.; Ishida, M.; Nakano, A.; Someya, S.; Munakata, T. Application of a self-supporting micro-porous layer to gas diffusion layers of proton exchange membrane fuel cells. *J. Power Sources* **2017**, *342*, 393–404. [[CrossRef](#)]
15. Mishra, A.K.; Bose, S.; Kuila, T.; Kim, N.H.; Lee, J.H. Silicate-based polymer-nanocomposite membranes for polymer electrolyte membrane fuel cells. *Prog. Polym. Sci.* **2012**, *37*, 842–869. [[CrossRef](#)]
16. Chien, H.C.; Tsai, L.D.; Lai, C.M.; Lin, J.N.; Zhu, C.Y.; Chang, F.C. Characteristics of high-water-uptake activated carbon/Nafion hybrid membranes for proton exchange membrane fuel cells. *J. Power Sources* **2013**, *226*, 87–93. [[CrossRef](#)]
17. Kim, H.; Kim, K. Numerical study on the effects of gas humidity on proton-exchange membrane fuel cell performance. *Int. J. Hydrog. Energy* **2016**, *41*, 11776–11783. [[CrossRef](#)]
18. Liu, J.X.; Guo, H.; Ye, F.; Ma, C.F. Two-dimensional analytical model of a proton exchange membrane fuel cell. *Energy* **2017**, *119*, 299–308.
19. Kahraman, H.; Orhan, M.F. Flow field bipolar plates in a proton exchange membrane fuel cell: Analysis & modeling. *Energy Convers. Manag.* **2017**, *133*, 363–384.
20. Zhang, X.; Wang, Y.; Liu, T.; Chen, J. Theoretical basis and performance optimization analysis of a solid oxide fuel cell-gas turbine hybrid system with fuel reforming. *Energy Convers. Manag.* **2014**, *86*, 1102–1109. [[CrossRef](#)]
21. Shin, Y.; Park, W.; Chang, J.; Park, J. Evaluation of the high temperature electrolysis of steam to produce hydrogen. *Int. J. Hydrog. Energy* **2007**, *32*, 1486–1491. [[CrossRef](#)]
22. Zhang, X.; Li, G.; Li, J.; Feng, Z. Numerical study on electric characteristics of solid oxide fuel cells. *Energy Convers. Manag.* **2007**, *48*, 977–989. [[CrossRef](#)]
23. Strahl, S.; Costa-Castelló, R. Temperature control of open-cathode PEM fuel cells. *IFAC-PapersOnLine* **2017**, *50-1*, 11088–11093.
24. Zhang, X.; Ni, M.; He, W.; Dong, F. Theoretical analysis and optimum integration strategy of the PEM fuel cell and internal combustion engine hybrid system for vehicle applications. *Int. J. Energy Res.* **2015**, *39*, 1664–1672. [[CrossRef](#)]
25. Rowe, A.; Li, X. Mathematical modeling of proton exchange membrane fuel cells. *J. Power Sources* **2001**, *102*, 82–96. [[CrossRef](#)]
26. Zhang, Y.; Mawardi, A.; Pitchumani, R. Numerical studies on an air-breathing proton exchange membrane (PEM) fuel cell stack. *J. Power Sources* **2007**, *173*, 264–276. [[CrossRef](#)]
27. Zhang, X.; Guo, J.; Chen, J. The parametric optimum analysis of a proton exchange membrane (PEM) fuel cell and its load matching. *Energy* **2010**, *35*, 5294–5299. [[CrossRef](#)]
28. Chan, S.H.; Low, C.F.; Ding, O.L. Energy and exergy analysis of simple solid-oxide fuel-cell power systems. *J. Power Sources* **2002**, *103*, 188–200. [[CrossRef](#)]
29. Larminie, J.; Dicks, A. *Fuel Cell Systems Explained*; Wiley: New York, NY, USA, 2003.
30. Ay, M.; Midilli, A.; Dincer, I. Exergetic performance analysis of a PEM fuel cell. *Int. J. Energy Res.* **2006**, *30*, 307–321. [[CrossRef](#)]
31. Pukrushpan, J.; Stefanopoulou, A.; Peng, H. Modeling and control for PEM fuel cell stack system. In Proceedings of the American Control Conference, Anchorage, AK, USA, 8–10 May 2002; IEEE: Piscataway, NJ, USA, 2002.
32. Wang, Y.; Chen, K.; Mishler, J.; Cho, S.; Adroher, X. A review of polymer electrolyte membrane fuel cells: Technology, applications, and needs on fundamental research. *Appl. Energy* **2011**, *88*, 981–1007. [[CrossRef](#)]

